ELSEVIER

Contents lists available at ScienceDirect

Dendrochronologia

journal homepage: www.elsevier.com/locate/dendro



Pan-alpine summer temperatures since 742 CE

Jan Esper ^{a,b,*}, Frederick Reinig ^a, Max Torbenson ^a, Edurne Martinez del Castillo ^a, Marcel Kunz ^a, Alberto Arzac ^c, Marco Carrer ^d, Feng Chen ^{e,f,g}, Alper K. Kadioglu ^{h,i}, Alexander V. Kirdyanov ^{c,j}, Ernesto Tejedor ^k, Mirek Trnka ^{b,l}, Ulf Büntgen ^{b,h,m}

- ^a Department of Geography, Johannes Gutenberg University, Mainz, Germany
- ^b Global Change Research Institute of the Czech Academy of Sciences, Brno, Czech Republic
- ^c Siberian Federal University, Krasnoyarsk, Russian Federation
- d Department of Land Environment Agriculture and Forestry, University of Padova, Legnaro, Italy
- ^e Institute of International Rivers and Eco-Security, Yunnan University, Kunming, People's Republic of China
- ^f Institute of Desert Meteorology, Chinese Meteorological Administration, Urumqi, People's Republic of China
- ^g Southwest United Graduate School, Kunming, People's Republic of China
- h Department of Geography, University of Cambridge, Cambridge, UK
- ⁱ Department of Forest Botany, Faculty of Forestry, Istanbul University Cerrahpasa, Istanbul, Turkiye
- ^j Sukachev Institute of Forest SB RAS, Federal Research Center, Krasnoyarsk, Russian Federation
- k Department of Geology, National Museum of Natural Sciences, Madrid, Spain
- ¹ Department of Agrosystems and Bioclimatology, Mendel University, Brno, Czech Republic
- ^m Department of Geography, Masaryk University, Brno, Czech Republic

ARTICLE INFO

Keywords: Climate reconstruction European Alps Larix decidua Maximum latewood density MXD Paleoclimate

ABSTRACT

Albeit labor-intensive, tree-ring maximum latewood density (MXD) has become a prime proxy to reconstruct inter-annual to multi-centennial climate variability. We here combine such data from five valleys in Austria, France and Switzerland to present a June-September temperature history for the European Alps reaching back to 742 CE. The pan-alpine record correlates at $r_{1880-2023}=0.89$ with observational data and provides evidence for a prolonged Little Ice Age (LIA) from the 1250s to 1850s CE, during which summer temperatures were 0.59 °C cooler compared to the preceding Medieval Warm Period (MWP) from the 880s to 1240s CE. Temperatures rose by 3.65 °C from the coldest decade in the 1810s, which includes the 1816 CE post-Tambora "year without a summer", to the warmest decade in the 2010s. The warmest summer in our reconstruction occurred in 2003 CE (+ 2.71 °C) and exceeds the warmest naturally forced summer in 970 CE (+ 2.19 °C) by more than 0.5 °C. This difference is non-significant, however, if we consider the increasing uncertainties back in time when fewer sites and trees contributed to the reconstruction. The pan-alpine record is the result of conducting MXD measurements over the past two decades in Swiss and German laboratories and sets a new standard in terms of explained variance and pre-instrumental temperature variability estimation in the European Alps.

1. Introduction

In 2006 Büntgen et al. (hereafter Bün06) published a millennium-length June-September temperature reconstruction based on only maximum latewood density (MXD) data from old buildings and living trees in the Swiss Lötschen (Loe) and Simplon (Sim) valleys. The record has been widely recognized and cited more than 500-times as it explains more instrumental temperature variance than any alpine tree-ring width (TRW) based reconstruction (Büntgen et al., 2005), which are typically compromised by biological memory (Esper et al., 2015). Bün06

correlates at $r_{1818-2003}=0.69$ and $r_{1760-1817}=0.80$ against regional June-September temperatures, thereby reaching levels that in Europe are only known from northern treeline environments in Fennoscandia where millennium-length MXD, blue intensity, and even more expensive stable isotope and quantitative wood anatomy timeseries explain more than 50 % (equal to r>0.71) instrumental temperature variance (e.g., Björklund et al., 2014, 2023; Büntgen et al., 2011a; Esper et al., 2012; Grudd, 2008; Gunnarson, Linderholm, 2002; Linderholm and Gunnarson, 2019; Loader et al., 2013).

Since most old buildings in the Swiss mountains are constructed of

Received 20 June 2025; Received in revised form 7 October 2025; Accepted 10 October 2025 Available online 12 October 2025

1125-7865/© 2025 The Author(s). Published by Elsevier GmbH. This is an open access article under the CC BY license (http://creativecommons.org/licenses/by/4.0/).

^{*} Corresponding author at: Department of Geography, Johannes Gutenberg University, Mainz, Germany. *E-mail address*: esper@uni-mainz.de (J. Esper).

durable Larix decidua Mill. wood, Bün06 had to adjust negative MXD outliers caused by defoliation events of regular larch budmoth (LBM) mass outbreaks (Johnson et al., 2010). The identification of these events in the Loe and Sim MXD data led to the longest reconstruction of regular insect outbreaks in subalpine environments (Esper et al., 2007a). The final Bün06 reconstruction was, however, still affected by a notable increase in variance during medieval times induced by highly covarying MXD series from single buildings in the Simplon valley. This bias, and potential inaccuracies caused by combining historical samples of unknown origin with well-confined living-tree collections (Tegel et al., 2010), stimulated an analysis of MXD signals along elevational transects and application of machine learning to improve tree provenancing and chronology building (Kuhl et al., 2024). The resulting temperature reconstruction, however, lacks centennial scale temperature trends and shows no evidence of a prolonged cold period associated with the Little Ice Age (LIA) that is otherwise commonly recorded in lower resolution proxy reconstructions from Central Europe and the European Alps (overview in Wanner et al., 2022).

We here address these limitations by introducing new high-elevation MXD datasets from the Swiss Lötschen and French Merveille valleys and combining these with existing data from the Swiss Matter and Simplon and the Austrian Ötz valleys. We develop a single MXD chronology for each of these five valleys using detrending methods to preserve low frequency variance, assess covariance and climate signals within this network, and calculate a mean timeseries to represent warm season temperatures across the European Alps. The resulting pan-alpine temperature history, integrating 1064 MXD measurement series of a mean length of 198 years, is finally compared with existing millennium-length reconstructions to evaluate similarities and discrepancies in reconstructed temperature extremes, trends, and amplitudes.

2. Material and methods

2.1. Site and MXD data characteristics

The valleys hosting long MXD chronologies range from the French Maritime Alps (Merveille valley, hereafter: Mer) in the southwest to the Austrian Ötztal Alps (Ötz valley: Oet) in the northeast and include a cluster of three sites in the Swiss Valais Alps (Lötschen: Loe, Simplon: Sim, Matter: Mat) in the center (Fig. 1). The sampling conditions and wood collections differ substantially among these five valleys. In Loe, we used the original larch collection including material from historical buildings and treeline sites sampled in 2004 CE (Loe04; Büntgen et al., 2006) and combined these data with a new collection of living and relict material (i.e. deadwood on the ground) sampled in 2022 CE at the treeline (Loe22). The combined Loe data includes 244 radii of a mean length of 269 years from elevations ranging between 1700 and 2200 m a.s.l. and covers the period from 1258 to 2021 CE (Table 1).

The Sim data are similar to the early Loe04 collection as they also include material from historical buildings and subalpine living trees. However, the lower boundary of the construction wood source region is less-well confined and estimated to reach down to 1600 m a.s.l. (Riechelmann et al., 2013). Sim is the smallest dataset (163 radii, 201 years mean length) but extends furthest back in time to 735 CE. It also includes some of the heaviest wood samples as expressed by the overall highest MXD mean of 0.93 g/cm³ compared to 0.82–0.88 g/cm³ in the four other valleys (Table 1). The nearby Mat collection is even less coherent and combines living trees from subalpine larch sites with relict material from a variety of sources including historical buildings in several small settlements as well as higher-elevation glacier wood (Kuhl et al., 2024; Riechelmann et al., 2020). Mat includes 193 measurement series of a mean length of 221 years from elevations ranging between 1600 and 2400 m a.s.l. covering the period from 765 to 2018 CE.

The Austrian Oet collection is the only non-larch dataset, being

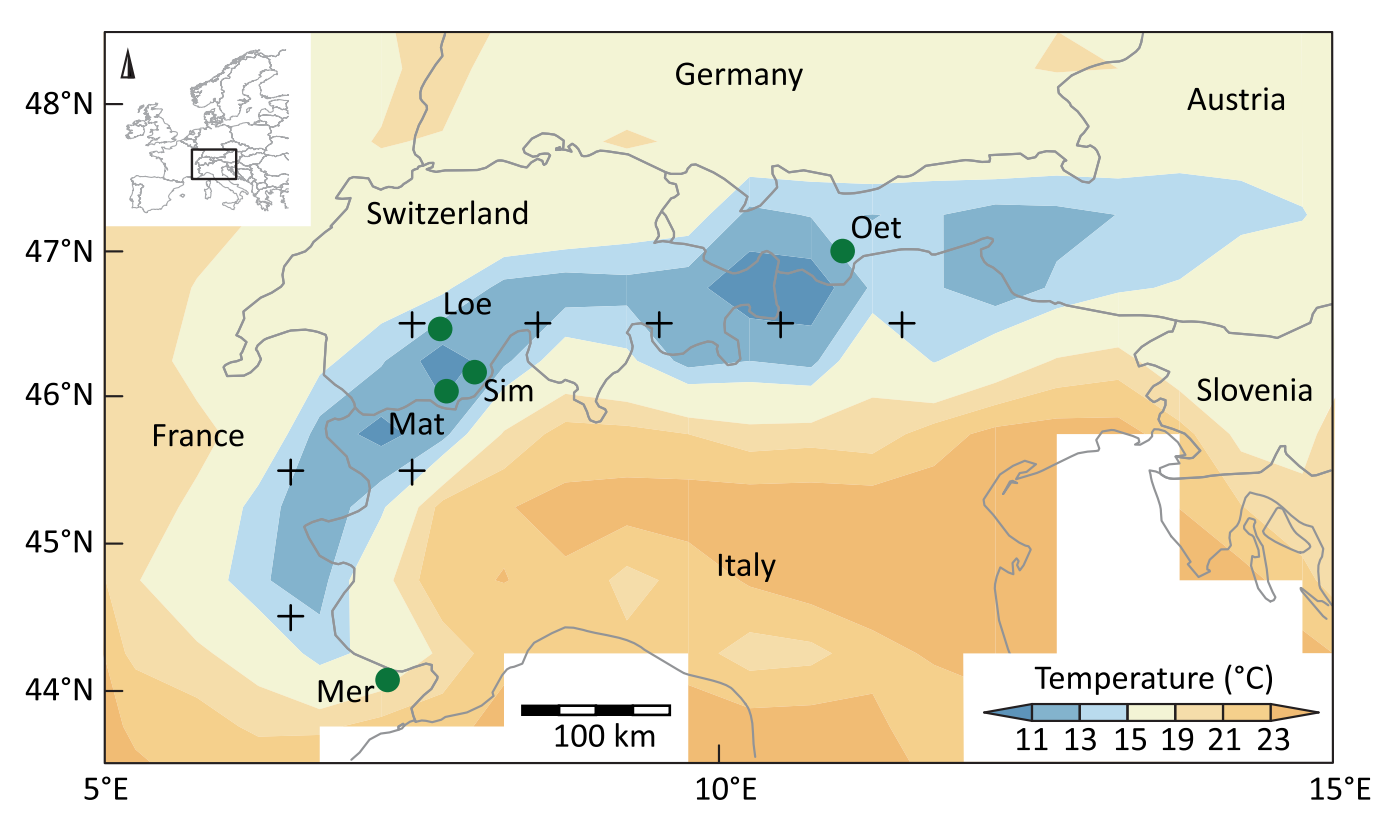


Fig. 1. Map showing the location of tree-ring density sites in the Lötschen (Loe), Simplon (Sim), Matter (Mat), Ötz (Oet), and Merveille (Mer) valleys (green dots), and observational temperature grid points (black crosses) in the European Alps. Background colors show the 2003 CE June-September temperatures using CRU TS 4.08 data (Harris et al., 2020).

Table 1
Site and MXD data characteristics. MSL is the mean segment length. Rbar is the inter-series correlation considering the 32-year spline detrending default in Cofecha (Holmes, 1983). JJAS signal is the Pearson correlation of a valley chronology with June–September mean temperatures since 1880 CE considering varying end dates.

	Loe	Sim	Mat	Oet	Mer
Lat./Lon.	46.40N, 7.80E	46.10N,8.00E	46.00N,7.70E	47.00N,11.00E	44.05N, 7.45E
Elevation [m]	1700-2200	1600-2100	1600-2400	1800-2000	2050-2350
Species	LADE	LADE	LADE	PCAB	LADE
Radii	244	163	193	205	259
Period	1258-2021 CE	735-2010 CE	765-2018 CE	1028-2003 CE	957-2023 CE
Length [yrs.]	764	1275	1253	976	939
MSL [yrs.]	269	201	221	129	166
Mean MXD [g/cm ³]	0.85	0.93	0.88	0.82	0.86
Rbar	0.63	0.57	0.60	0.61	0.50
JJAS signal	r = 0.85	r = 0.82	r = 0.77	r = 0.67	r = 0.74

composed of *Picea abies* living-tree and relict samples from a well-confined subalpine environment between 1800 and 2000 m a.s.l. The spruce samples are lighter than the larch, as expressed by the lowest MXD mean of 0.82 g/cm³, and have been reported to contain seasonal temperature signals that are more strongly weighted towards late summer months (Esper et al., 2007b). Oet includes 205 MXD series of relatively short length (129 years) covering a period from 1028 to 2003 CE. The most recently completed Mer dataset extends until 2023 CE and is composed of ground deadwood and living trees all from elevations above 2050 m a.s.l. Many of the deadwood samples are rather old and include up to 900 rings (Büntgen et al., 2012; Serre, 1978), whereas the living trees represent all age classes down to series shorter than 20 rings. Mer represents a total of 259 series of a mean length of 166 years extending back to 957 CE.

All data have been measured using Walesch X-ray densitometers in the Birmensdorf (Switzerland) and Mainz (Germany) tree-ring laboratories to produce high-resolution density profiles of more than 210,000 rings (Fig. 2). While time-consuming, this method enables quantification of intra-annual density metrics including MXD at highest precision even in narrow rings characteristic for high-elevation alpine environments. Due to changes in the densitometry calibration wedge and other, partly undocumented modifications, some of the early Sim measurements conducted in Birmensdorf are systematically lighter by 0.1 g/cm³ and had to be adjusted to the Mainz measurements before joint detrending.

2.2. Detrending and chronology building

We generally used simple RCS detrending (Briffa et al., 1992; Esper et al., 2003) with ratios and arithmetic means applied either to entire valley datasets or after splitting data into living-tree and dead-tree subsamples (Melvin et al., 2013). In Mat, we additionally used horizontal line detrending with a sub-sample of old trees to cope with the

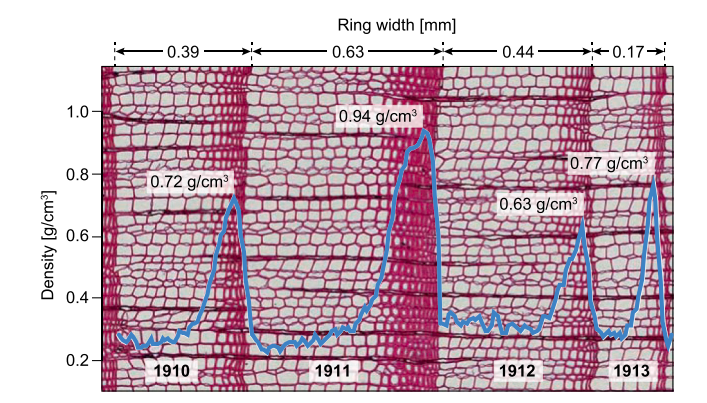


Fig. 2. Tree-ring width and density. Thin section showing the rings 1910–1913 CE of a larch tree in the Lötschen valley. The blue curve is the high-resolution density profile derived from X-ray densitometry with maximum latewood density (MXD) values highlighted towards the end of each ring.

highly variable relict data from various sources. MXD reductions caused by mass outbreaks of *Zeiraphera diniana* (Kunz et al., 2023) were removed from raw measurement series using an impulse indicator saturation algorithm (Pretis et al., 2017; "isat" function in "gets" R-package) together with the LBM-free MXD chronology developed for periodic mass infestation detection (Esper et al., 2007a; Supplementary Fig. S1). Additional tests using (i) residuals instead of ratios, (ii) robust instead of arithmetic means, and (iii) signal free RCS instead of RCS revealed no notable differences among chronologies. This lack of change results from the relatively flat age trends in MXD compared to TRW, in which even biologically old data remain distant from the X-axis (Schweingruber et al., 1979; Briffa et al., 1998; Frank and Esper, 2005; Esper et al., 2010).

In detail, we produced two RCS chronologies in the Lötschen valley, one using the combined historic and living-tree Loe04 collection as in Bün06, and a second one using the new Loe22 collection, consisting of only samples from the treeline. Notably, the Loe04 RCS chronology shows an overall stronger positive trend towards present (Supplementary Fig. S2), which is counterintuitive to impending biases that might arise from combining potentially heavier wood from lower elevation buildings with lighter living trees from higher elevations. We therefore used the mean of both RCS chronologies, LoeO4 and Loe22, to form a timeseries representing the Lötschen valley (Supplementary Fig. 3a). In Sim and Mer, we split the data into relict and living-tree subgroups and combined the resulting RCS chronologies to valley mean curves. This separation appeared necessary to mitigate potential biases from systematically heavier historical wood of unknown origin in Sim, and avoid the combination of very old deadwood with much younger living trees in one RCS run in Mer. In Mat, we detrended the relict subsample using horizontal means applied only to trees older than 100 years. This was done to support the combination of these highly variable data with RCS-detrended living trees. Comparable partitions were not necessary in Oet where the relict and living-tree samples are similarly old and from a well-confined environment, so that only one RCS run was conducted with these data.

All chronologies were truncated at a minimum replication of n=3 MXD series (except the combined Loe data at n=8) and their variance stabilized by calculating ratios from 100-year running standard deviations obtained from 30-year high-pass filtered timeseries to mitigate effects of temporally changing replication and covariance (Frank et al., 2007b). The five valley chronologies (Supplementary Fig. S3) were normalized and averaged to produce an alpine mean (V5M) and the covariance among chronologies assessed using 100-year running correlations.

2.3. Instrumental temperatures and MXD calibration

We used Berkeley Earth $1^{\circ}x1^{\circ}$ gridded temperatures back to 1750 CE for proxy calibration (Rohde et al., 2013). Comparison of June–September means from various locations (see crosses in Fig. 1) reveals a highly coherent temperature field across the European Alps at an

interseries correlation $\operatorname{Rbar}_{1750-2022} = 0.98$ (Fig. 3) justifying the linear combination of valley chronologies and reconstruction of pan-alpine conditions. Covariance among temperature timeseries declines back in time though, which is the result of fewer (and more remote) station records contributing to the single grid points. This tendency is additionally fueled by an increasing warming trend towards present and punctuated by major volcanic eruptions of Tambora in 1815 CE and Novarupta in 1912 CE (Fig. 3b).

Considering these characteristics of the target temperature field, we decided to (i) develop a single MXD record integrating the information of five alpine valleys, (ii) calibrate this record against instrumental data since 1880 CE, and (iii) use the early observational data from 1750 to 1879 CE for extra verification. Validity of this approach is exemplified by highly coherent MXD variations across the five-valley network in response to distinct temperature variations from 1910 to 1913 CE (highlighted in red in Fig. 3b) during which June-September means dropped by more than 3 $^{\circ}\text{C}$ from 1.35 $^{\circ}\text{C}$ in 1911 CE to - 2.03 $^{\circ}\text{C}$ in 1912°C. While 1911 CE coincided with a strong El Niño event (Wang et al., 2019), the massive high latitude eruption of Novarupta in early June 1912 (Hildreth and Fierstein, 2012) triggered the following summer cooling and produced a temperature zigzag that is closely captured by the 324 series of the pan-alpine MXD network (Fig. 4). The corresponding TRW series, however, appear less coherent and affected by biological memory (Esper et al., 2015), justifying the focus on MXD for temperature reconstruction.

The five valley chronologies and their V5M mean were correlated with monthly and seasonal temperatures of the 6.5°E/44.5°N grid point. The V5M signal was additionally assessed in a split-period 1880-1951 CE versus 1952-2023 CE calibration/verification approach and the proxy data linearly regressed against seasonal temperatures to compute conventional RE and CE statistics (Cook et al., 1994). We additionally removed low frequency variance from the MXD and instrumental data using 10-year high-pass filters to compare modelled and recorded temperature amplitude changes back to 1750 CE. For the final reconstruction, V5M was scaled (Esper et al., 2005) against June-September mean temperatures over the full 144-year calibration period from 1880 to 2023 CE, and uncertainties were estimated by calculating calibration standard errors (SE) in a nesting approach combining valley chronologies of varying length (Wilson et al., 2016). The resulting series were smoothed using a 30-year filter to visualize changes over the past 1282 years back to 742 CE.

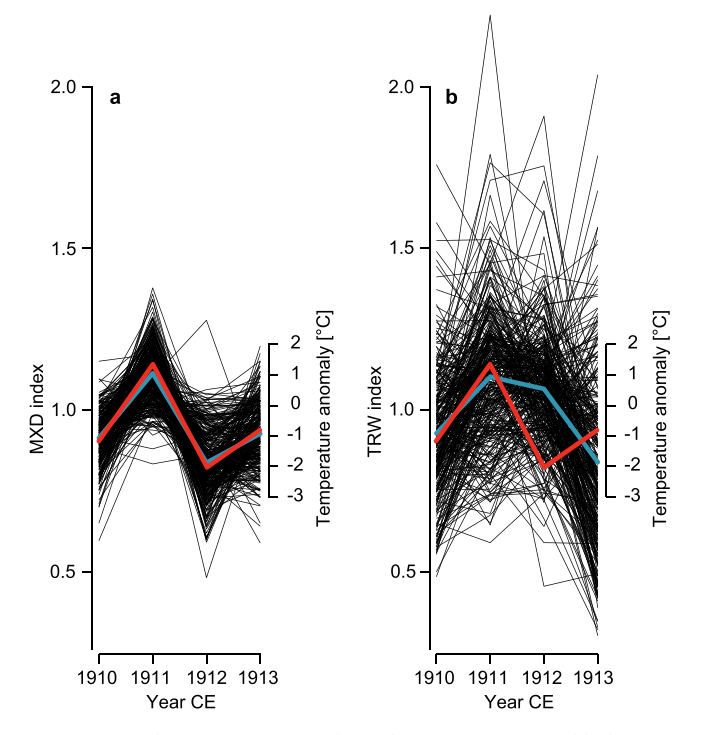


Fig. 4. MXD and TRW covariance and signal. **a**, 324 MXD series (black curves) and their arithmetic mean (blue) shown together with instrumental June-September temperature anomalies (red, grid point $6.5^{\circ}\text{E}/44.5^{\circ}\text{N}$, anomalies with respect to 1951–1980 CE) from 1910 to 1913 CE. **b**, Same as in **a**, but for TRW. All tree-ring series were detrended using 30-year splines.

3. Results and discussion

3.1. Alpine valley MXD chronologies

The five valley chronologies share common high-to-low frequency variability including a long-term decrease from the mid 11th to the early 14th centuries and a long-term increase since the early 19th century (Fig. 5). These multi-centennial trends frame a period from the mid 13th to the early 19th centuries, during which the chronologies show overall lower values. These coherent, lowest frequency trends have been retained in all MXD chronologies even though the age structure, source material, sampling elevations, split procedures, detrending, and tree

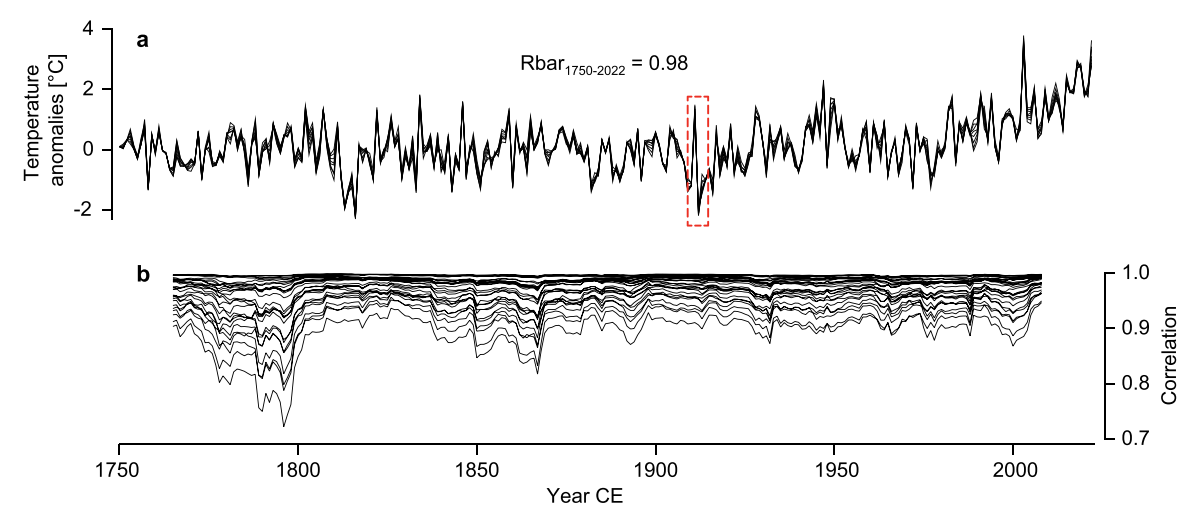


Fig. 3. Instrumental temperatures. a, Berkeley Earth (Rohde et al., 2013) June-September mean temperature anomalies (with respect to 1951–1980) at eight grid points across the European Alps (see crosses in Fig. 1). The red dashed box highlights the years 1910–1913 CE shown in detail in Fig. 4. b, Centered 30-year running correlations between the grid point temperatures back to 1750 CE.

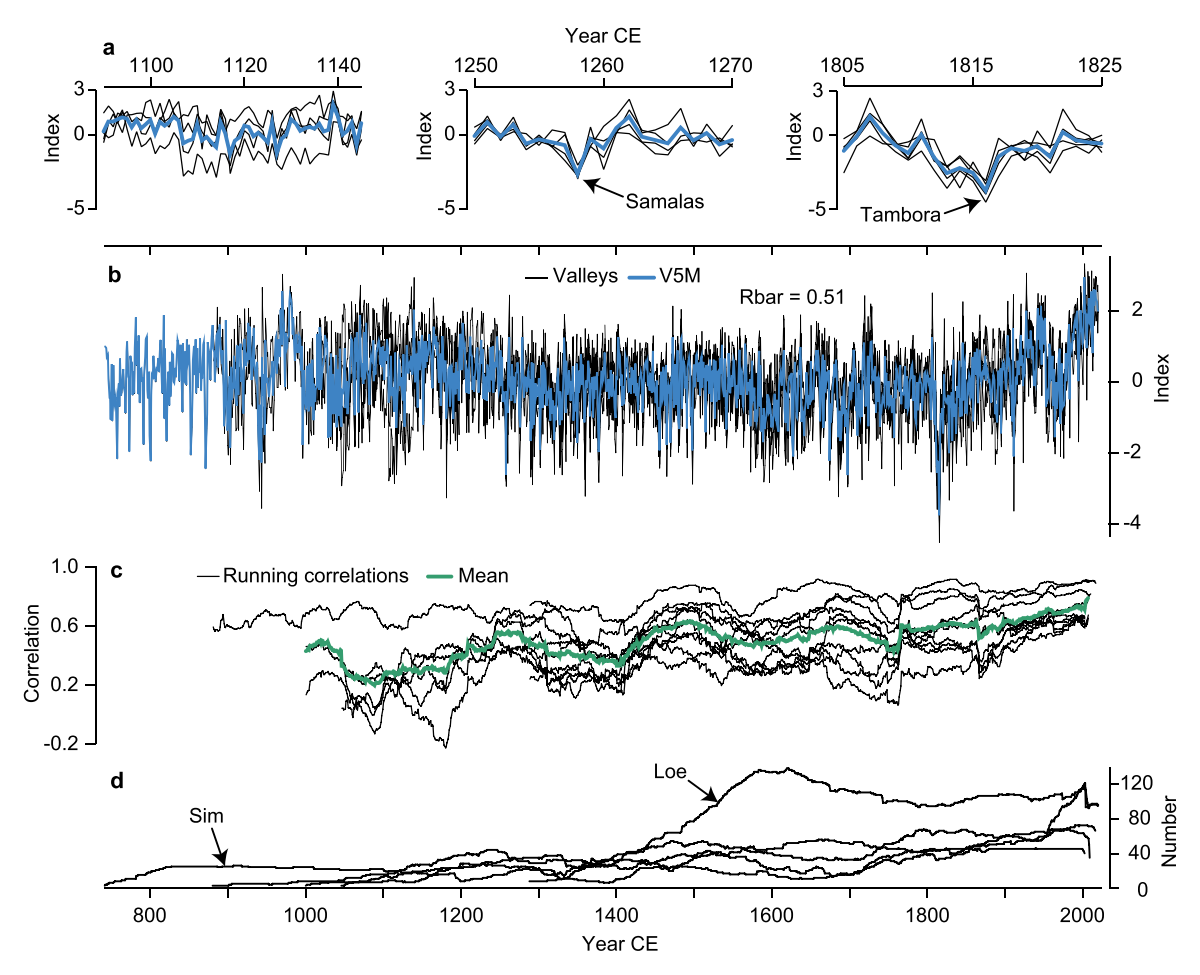


Fig. 5. Alpine valley MXD chronologies. a, Zoom-ins showing the chronologies (black) and V5M mean (blue) from 1090 to 1145 CE, 1250–1270 CE, and 1805–1825 CE. b, Normalized Loe, Sim, Mat, Oet, and Mer chronologies (black) and their V5M mean (blue) since 742 CE. Rbar is the interseries correlation among all records. c, 100-year running correlations (50-year towards the ends) between chronology pairs (black), and their mean (green). d, Changing numbers of MXD series included in the valley MXD chronologies.

species differ fundamentally among the valleys. Besides differing absolute densities, the long-term trends in index chronologies originate from varying MXD age trends as illustrated in the age-aligned regional curves of the living-tree versus relict-tree larch collections (Supplementary Fig. S4).

The valley chronologies also covary at interannual-to-multi-decadal scales, yet their Rbar of 0.51 is much lower compared to the gridded alpine temperatures (Fig. 3). Pairwise correlations range from r=0.76 and r=0.74 between the nearby Loe and Mat, and Loe and Sim valleys, respectively, to r=0.34 between the remote Oet and Mer valleys, calculated over their 1289–2003 CE common period. The difference among valley records is largest from 1100 to 1140 CE (highlighted in Fig. 5a) when the French Mer chronology is substantially lower compared to Sim, Mat, and Oet. The chronologies are, on the other hand, highly coherent during periods of massive tropical eruptions, such as Tambora in 1815 CE and Samalas in 1257 CE that triggered the two most negative deviations in the V5M mean over the past 1282 years.

These characteristics, in addition to the increased agreement associated with post-1900 CE greenhouse gas forced warming and the solar forced Maunder Minimum culminating in the late 17th century, are all reflected in the network running correlations (Fig. 5c). Most striking, however, is the general decline in covariance back over the past millennium, which is driven by the shrinking MXD replication of valley chronologies and the alpine network as a whole (Fig. 5d). This feature is characteristic of every tree-ring based climate reconstruction (Esper et al., 2016; Ljungqvist et al., 2020) but remains challenging to translate into meaningful uncertainties, particularly when combining predictors

from various locations (e.g., Anchukaitis and Smerdon, 2022; Anchukaitis et al., 2017; Cook et al., 2024; Esper et al., 2018, 2024a; Frank et al., 2010; Tejedor et al., 2020). For the alpine MXD network and any reconstruction derived from these data, it means that the earlier deviations and trends are less certain even if the same number of valley chronologies are averaged. When, in addition, valley chronologies drop out (such as Loe in 1289 CE, Oet in 1047, Mer in 1001 CE, and Mat in 881 CE) uncertainty steps up, which is here accounted for by iteratively calibrating valley chronology means in a nesting approach (see below; Wilson et al., 2016). More sophisticated methods to estimate uncertainty could be applied though.

3.2. MXD climate signals

The seasonal climate signal of the valley chronologies and V5M peaks in August and reaches a maximum when averaging June-September temperatures (Supplementary Fig. S5). Besides minor differences among the four larch collections, the Oet spruce chronology shows a seasonally delayed response culminating in August and September. However, adding this record to the alpine mean generally increases calibration statistics, and adjusting the seasonality to fully account for the sensitivity of the Oet data would be an unnecessary complication of the reconstruction approach. We therefore targeted June-September temperatures to calibrate and scale the V5M mean.

V5M correlates at r=0.89 with June-September mean temperatures since 1880 CE (Fig. 6), thereby exceeding the score of any tree-ring based climate reconstruction in Europe. The record performs equally

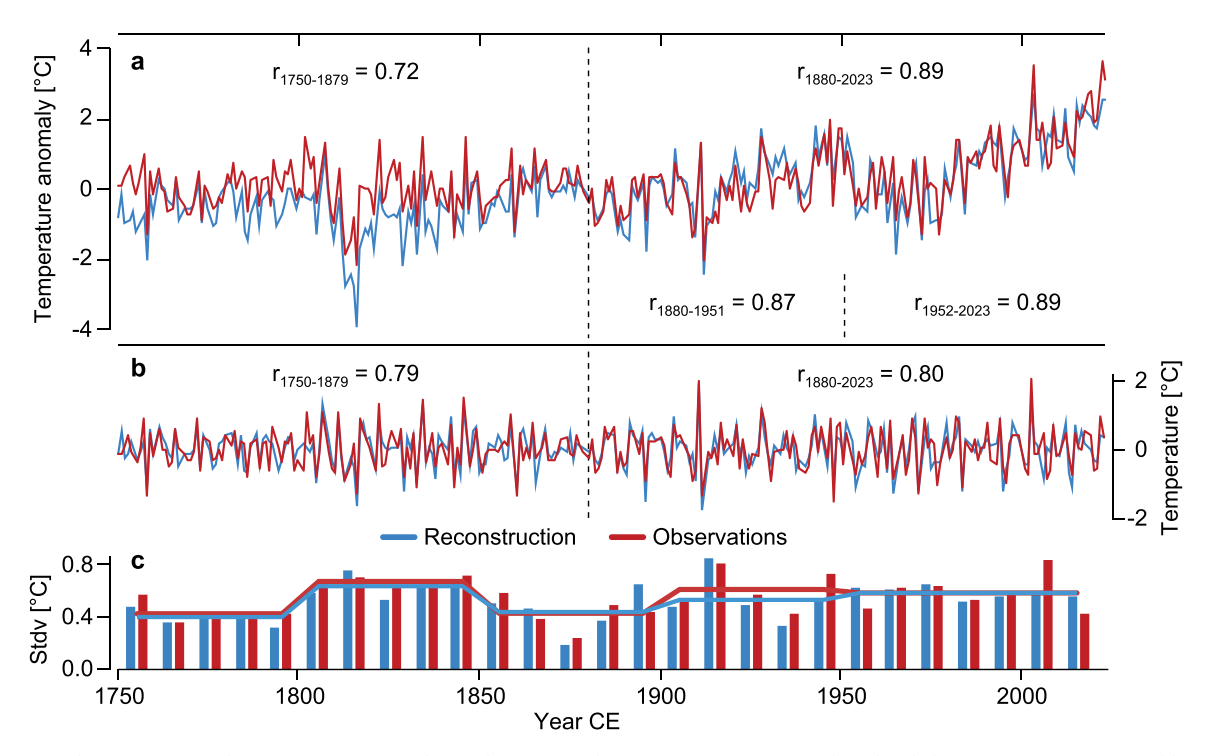


Fig. 6. Proxy signal. a, June–September temperature anomalies with respect to the 1951–1980 CE mean (red) and scaled PAN-ALP reconstruction (blue) since 1750 CE. b, Same as in a, but shown as residuals from 10-year Gaussian filters. c, Ten-year (histogram) and 50-year (curves) standard deviations of the high-pass filtered data shown in b.

well over the early and late calibration/verification periods reaching RE and CE scores ranging from 0.71 to 0.79 and 0.59 to 0.67, respectively. V5M even correlates at r=0.72 over the extra verification period prior to 1880 CE during which the instrumental network is composed of only a few station readings (Auer et al., 2007). This period is also characterized by an offset between warmer instrumental and colder proxy data that has previously been identified and attributed to direct insolation effects on insufficiently sheltered thermometers (Böhm et al., 2010; Frank et al., 2007a; Schneider et al., 2023) and is here considered by scaling V5M over the 1880–2023 CE period to produce the PAN-ALP June-September temperature reconstruction.

The early instrumental offset (ΔT) is particularly striking in 1816 CE when the MXD-based estimate is - 1.77 °C colder than the thermometer readings. While we argue that PAN-ALP is superior to any instrumental figure during this biased period, recent offsets such as in 2003 CE ($\Delta T = -0.82$ °C) and 2022 CE ($\Delta T = -1.09$ °C) require different attribution. In 2003 CE, which was particularly hot during early summer, a seasonal miss-match with the late summer-weighted MXD data likely contributed to the offset. In 2022 CE, the offset may be affected by the reduced network replication to only one valley (Mer) despite striking MXD covariance during recent decades. However, taking these incidents together, the record-breaking summer of 2003 and subsequent hot years may also mark a threshold for stationary responses beyond which MXD does not fully capture the predictand's variance. This is simply because the sampling sites fell too far below the rapidly rising potential treeline (Büntgen et al., 2022). More research is needed to clarify this.

PAN-ALP stationarity and skill is reinforced by comparing the highpass filtered observational and proxy data scoring r=0.79 and r=0.80 prior and after 1880 CE, respectively (Fig. 6b). This experiment not only indicates that greenhouse gas forced warming increased recent correlations in the original, non-detrended data (values in Fig. 6a), but emphasizes the close resemblance of temperature amplitude changes back to 1750 CE (Fig. 6c). The skill to capture multi-decadal predictand variance changes is a fundamental limitation of tree-ring research as the heteroscedastic nature of TRW forces dendroclimatologists to adjust and even variance in detrended index series (Bräker, 1981; Cook and

Kairiukstis, 1990). This shortcoming is mitigated in MXD as these measurements hardly contain any spread-versus-level relationship (Cook, Peters, 1997; Esper et al., 2003). However, as with all other tree-ring proxies, the variance of mean chronologies needs to be adjusted to account for changes in replication and Rbar (Frank et al., 2007b), which is here achieved by calculating ratios from 100-year running standard deviations of 30-year high-pass filtered data. The long PAN-ALP reconstruction therefore has skill in retaining variance changes at decadal to multi-decadal scales but is limited beyond these periods.

3.3. Pan-alpine temperature reconstruction

The spatial PAN-ALP signal is weighted westward into the Mediterranean (Supplementary Fig. S6) and the record shows rich inter-annual to multi-centennial temperature variability (Fig. 7). The coldest summers occurred in 1816 and 1258 CE following the two largest volcanic eruptions of the past millennium (Toohey and Sigl, 2017), and the absolute temperature range between these extremes and the greenhouse gas forced summer of 2003 CE exceeds 6.5 °C (Table 2). Note though that the reconstructed temperatures underestimate warmth during 2003 CE but overestimate cold during 1816 CE as discussed above. PAN-ALP shows that 2003 CE was more than 0.5 $^{\circ}\text{C}$ warmer than the warmest naturally forced summer in 970 CE thereby providing a first-order idea of the contribution of anthropogenic greenhouse gases against background climate forcing over more than 1000 years. Such comparisons are, however, constrained by the 95 % uncertainties of the pan-alpine reconstruction estimated to range $\pm\,0.95\,^{\circ}\text{C}$ back to 1289 CE and \pm 1.16 °C before 881 CE (thin blue curves in Fig. 7).

Pan-alpine temperatures were almost 0.6 °C warmer during the MWP compared to the LIA (Table 2), yet the transition between these major climate states centered during the 13th century remains largely unexplained. Bradley et al. (2016) suggested that a relative lack of volcanic eruptions contributed to medieval warmth, and a period of larger eruptions starting in 1257 CE with Samalas persistently altered this forcing. However, while Samalas indeed triggered a substantially

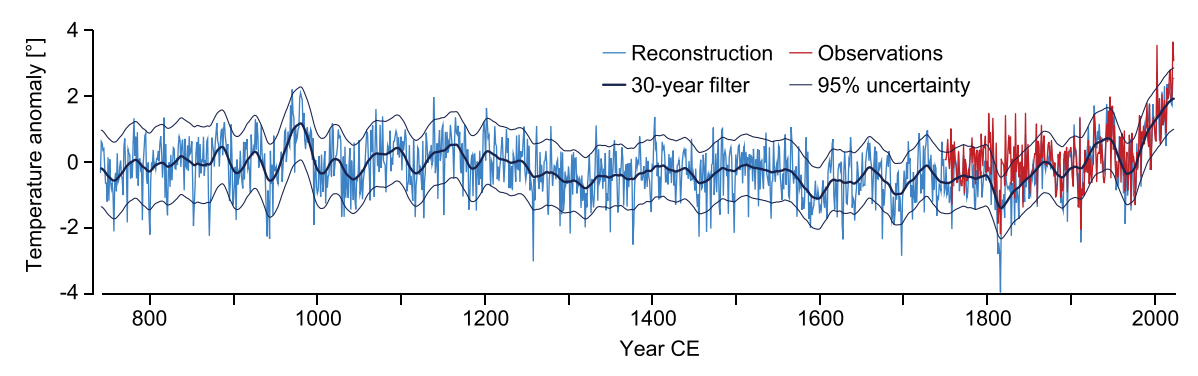


Fig. 7. Alpine June-September temperature reconstruction from 742 to 2023 CE (blue curve). Thick curve is a 30-year Gaussian filter and thin curves indicate the smoothed two standard error range derived from nested calibration of five valley chronologies against observational temperatures (red curve) since 1880 CE. All data expressed as anomalies with respect to the 1951–1980 CE mean.

Table 2
Mean June–September temperature anomalies (with respect to 1951–1980 CE) during the warmest and coldest reconstructed years, decades, Medieval Warm Period (MWP), Little Ice Age (LIA), and Recent Warming (RW) periods.

	Year	JJAS temp.	Decade	JJAS temp.	Period	JJAS temp.
Warmest	2003 CE	2.71 °C	2010s	1.75 °C	MWP	
	2022 CE	2.53 °C	2000s	1.50 °C	880-1240s	0.10 °C
	970 CE*	2.19 °C	970s	1.11 °C	LIA	
Coldest	1816 CE	− 3.94 °C	1810s	− 1.90 °C	1250-1850s	− 0.49 °C
	1258 CE	− 3.00 °C	1590s	− 1.16 °C	RW	
	1698 CE	– 2.83 C	1690s	– 1.12 C	since 1860s	0.37 °C

^{* 970} CE is the 7th warmest summer. All others occurred after 2011.

cold summer (-3.00 $^{\circ}$ C in 1258 CE), PAN-ALP shows that cooling had already started in the late 12th and early 13th centuries, long before this major eruption and the subsequent solar Wolf minimum (Usoskin, 2017). Earlier eruptions, such as in 1108, 1171, and 1230 CE (Sigl et al., 2015) left no notable fingerprint in the European Alps.

The coldest reconstructed decades, ranging from -1.12 to $-1.90\,^{\circ}$ C, occurred more than 300 years later in the late 16th, 17th, and early 19th centuries (Table 2). While forcing of the first of these periods remains unclear, the 1690s cold coincided with the exceptional solar Maunder Minimum (Usoskin, 2017) and the 1810s with the 1809 CE unknown and 1815 CE Tambora eruptions (Gao et al., 2023). Subsequent to the 1810s PAN-ALP low point, substantial warming already started in the first half of the 19th century, long before the accumulation of anthropogenic greenhouse gases in the atmosphere fundamentally altered Earth's radiation budget (King et al., 2015). The effects of this forcing became clearly visible in 2003, 2022, and 2023 CE, when summer temperatures exceeded those of the MWP, even if we consider the smoothed uncertainty estimates.

3.4. Reconstruction benchmarking

Comparison of PAN-ALP with the widely recognized Bün06 reconstruction reveals coherent post-1200 CE decadal to multi-centennial trends, but substantial differences before (Fig. 8a and b). While the reconstructed temperature amplitude is overall similar (see arrows on the right of Fig. 8), the 3.4 °C recorded in the smoothed Bün06 data arise from a very cold LIA, which may be overemphasized in the combined historical and living-tree collection from the Swiss Lötschen valley (Supplementary Fig. S1). The 3.3 °C amplitude of PAN-ALP is, on the other hand, driven by the exceptional warming during recent decades (Esper et al., 2024b; Tejedor et al., 2024) retained in this updated timeseries until 2023 CE. The differences prior to 1200 CE result from the integration of different valleys in PAN-ALP and adjustment of variance during early, less-replicated chronology sections. PAN-ALP temperatures during MWP fluctuated around the 1951–1980 CE mean, and the 30-year period of maximum warmth from 965 to 994 CE (+ 1.18 °C)

is clearly exceeded by current conditions reaching $+\ 1.53\ ^{\circ}C$ since 1994 CE. The same 30-year MWP period is also prominent in the Kuhl et al. (2024) provenanced reconstruction (Fig. 8c) that uses some of the same MXD data from the Swiss Simplon and Matter valleys as Bün06 and this study. However, the provenanced reconstruction lacks any evidence of a LIA in the European Alps, and recent warming does not exceed the MWP, two conclusions that appear unrealistic in light of the new pan-alpine but also other reconstructions.

Similar discrepancies are seen in the TRW-based reconstruction from the Austrian Alps (Büntgen et al., 2011b), which together with the TRW-based reconstruction from the Swiss Alps (Büntgen et al., 2005) indicate larger temperature amplitudes of 3.9 °C and 4.4 °C over the past millennium, respectively (Fig. 8d and e). Exaggerated fluctuations have already been attributed by the original authors to biological memory effects in TRW data and were part of our motivation to continue producing expensive MXD data over the past years. The generally synchronous inter-decadal variations observed in other valleys, species, and tree-ring parameters are viewed as supportive evidence that the fluctuations recorded in the pan-alpine PAN-ALP reconstruction are climatically meaningful. This interpretation also applies to the TRW-based reconstruction from the French Alps (Fig. 8f), even though many of the MXD measurement series included in PAN-ALP are from the same relict wood samples (Serre, 1978).

Data overlap among tree-ring reconstructions justifies additional comparisons with lower resolution proxies, such as the chironomid-based temperature reconstruction from the Swiss Engadin (Larocque-Tobler et al., 2010), even though the dating and calibration of such archives does not meet dendrochronological standards (Fig. 8g). The 4.5 °C temperature amplitude of the lake sediment record appears excessive, particularly as the data do not extend until present and therefore miss current warming. The reconstruction also shows no cold conditions during the early 19th century, which is a dominant feature in all other reconstructions and early instrumental data. However, it does show prolonged cold conditions associated with the LIA and perhaps most importantly a pronounced cooling trend from the late 12th to the late 14th centuries, just like PAN-ALP. The MXD-based reconstruction,

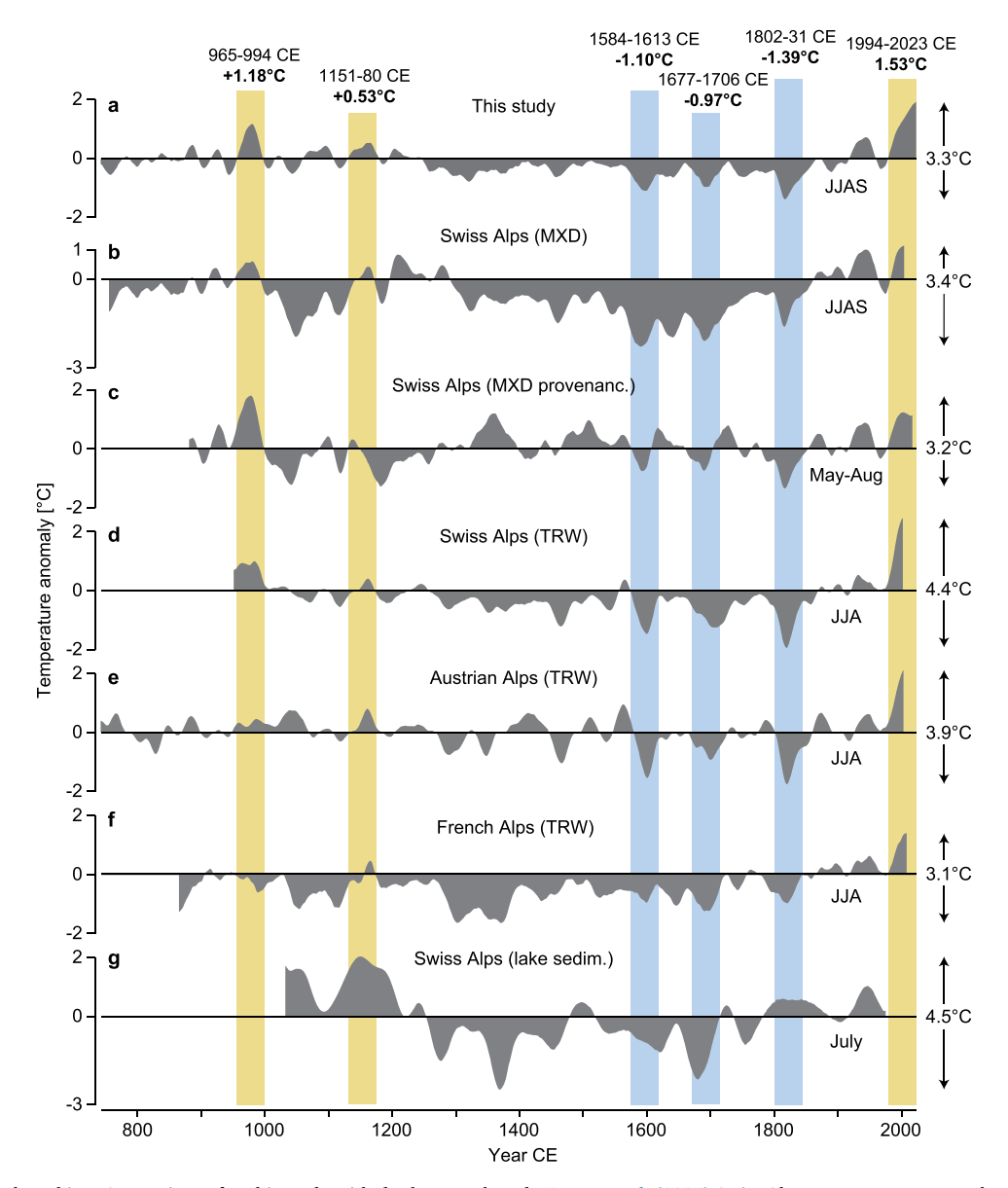


Fig. 8. PAN-ALP benchmarking. Comparison of a, this study with, b, the MXD-based Büntgen et al. (2006) Swiss Alps, c, MXD provenance-based Kuhl et al. (2024) Swiss Alps, d, TRW-based Büntgen et al. (2005) Swiss Alps, e, TRW-based Büntgen et al. (2011b) Austrian Alps; f, TRW-based Guillet et al. (2017) French Alps, and g, lake sediment-based Larocque-Tobler et al. (2010) Swiss Alps temperature reconstructions, all scaled since 1880 CE against June-September instrumental temperature anomalies (with respect to 1951–1980 CE) and smoothed using 30-year Gaussian filters. Temperature signals range from June-September (JJAS), to May-August (MJJA), June-August (JJA), and July. Exceptionally warm and cold 30-year periods highlighted in yellow and blue, respectively.

however, shows that the temperature amplitude of this transition was much smaller than indicated in the Swiss lake sediment data.

4. Conclusions

The combination of MXD data from five valleys in Austria, Switzerland, and France enabled the development of a 1282-year June-September temperature history (PAN-ALP) that calibrates better than any other reconstruction from Europe. Addressing pan-alpine climate with a single record appeared justified as state-of-the-art gridded temperatures correlate at $\rm r=0.98$ across the European Alps. PAN-ALP does not rewrite the temperature history of the European Alps but adds a new level of precision to the estimation of pre-instrumental trends and variance changes over the past millennium. It shows that current warming exceeds the envelope of natural climate variability and refines our understanding of the MWP when temperatures fluctuated around the 1951–1980 CE climatological mean. The climate signal and shape of

the pan-alpine reconstruction are fairly robust, i.e. would be similar if other methods for chronology building, network aggregation, and transfer were applied. This is because MXD age trends are rather small (typically $<0.2~{\rm g/cm^3})$ and inter-annual MXD variability unaffected by biological memory. Reconstruction uncertainty increases back in time, however, as the number of MXD measurement series and sites declines and is here estimated to exceed $\pm\,1~^{\circ}\text{C}$ before 1047 CE. Funding of projects intending to produce MXD, but also stable isotope and quantitative wood anatomy measurements, preferably from relict wood and old buildings, is therefore recommended.

CRediT authorship contribution statement

Alberto Arzac: Writing – review & editing, Resources, Data curation. Marcel Kunz: Writing – review & editing, Formal analysis. Edurne Martinez del Castillo: Writing – review & editing, Investigation, Data curation. Kirdyanov Alexander: Writing – review & editing,

J. Esper et al. Dendrochronologia 94 (2025) 126432

Validation, Methodology. Kadioglu Alper: Writing – review & editing, Investigation. Feng Chen: Writing – review & editing, Validation, Investigation. Marco Carrer: Writing – review & editing, Validation, Data curation. Max Torbenson: Writing – review & editing, Validation, Methodology. Ulf Büntgen: Writing – review & editing, Investigation, Data curation, Conceptualization. Frederick Reinig: Writing – review & editing, Validation, Data curation. Mirek Trnka: Writing – review & editing, Funding acquisition. Jan Esper: Writing – review & editing, Formal analysis, Conceptualization. Ernesto Tejedor: Writing – review & editing, Methodology, Formal analysis.

Declaration of Competing Interest

The authors declare that they have no known competing financial interests or personal relationships that could have appeared to influence the work reported in this paper.

Acknowledgements

Supported by the ERC Advanced Grant MONOSTAR (AdG 882727), the ERC Synergy project SYNERGY-PLAGUE (101118880), the cofunded EU project AdAgriF (CZ.02.01.01/00/22_008/0004635), and the German Science Foundation Project ES 161/15-1 on wood density methods. ET received funding from the Comunidad de Madrid program Atracción Talento "César Nombela" (2023-T1/ECO-29118). We are thankful to the staff who produced the MXD data over the past decades, including Anne Verstege, Daniel Nievergelt, Markus Kochbeck, Jutta Sonnberg, and Birgit Wöste.

Appendix A. Supporting information

Supplementary data associated with this article can be found in the online version at doi:10.1016/j.dendro.2025.126432.

Data availability

Data will be made available on request.

References

- Anchukaitis, K.J., Smerdon, J.E., 2022. Progress and uncertainties in global and hemispheric temperature reconstructions of the common era. Quat. Sci. Rev. 286, 107537.
- Anchukaitis, K.J., Wilson, R., Briffa, K.R., Büntgen, U., Cook, E.R., D'Arrigo, R., Zorita, E., 2017. Last millennium Northern hemisphere summer temperatures from tree rings: Part II, spatially resolved reconstructions. Quat. Sci. Rev. 163, 1–22.
- Auer, I., Böhm, R., Jurkovic, A., Lipa, W., Orlik, A., Potzmann, R., Nieplova, E., 2007. HISTALP – historical instrumental climatological surface time series of the greater Alpine region. Int. J. Clim. 27, 17–46.
- Björklund, J., Seftigen, K., Stoffel, M., Fonti, M.V., Kottlow, S., Frank, D.C., von Arx, G., 2023. Fennoscandian tree-ring anatomy shows a warmer modern than medieval climate. Nature 620, 97–103.
- Björklund, J.A., Gunnarson, B.E., Seftigen, K., Esper, J., Linderholm, H.W., 2014. Blue intensity and density from Northern fennoscandian tree rings, exploring the potential to improve summer temperature reconstructions with earlywood information. Clim 10, 877–885.
- Böhm, R., Jones, P.D., Hiebl, J., Frank, D., Brunetti, M., Maugeri, M., 2010. The early instrumental warm-bias: a solution for long central European temperature series 1760–2007. Clim. Change 101, 41–67.
- Bradley, R.S., Wanner, H., Diaz, H.F., 2016. The medieval quiet period. Holocene 26, 990–993.
- Bräker, O.U., 1981. Der alterstrend bei Jahrringdichten und Jahrringbreiten von Nadelhözern und sein Ausgleich. Mitte Forstl. Bundes-Vers. Wien. 142, 75–102.
- Briffa, K.R., Jones, P.D., Bartholin, T.S., Eckstein, D., Schweingruber, F.H., Karlen, W., Eronen, M., 1992. Fennoscandian summers from AD 500: temperature changes on short and long timescales. Clim. Dyn. 7, 111–119.
- Briffa, K.R., Jones, P.D., Schweingruber, F.H., Osborn, T.J., 1998. Influence of volcanic eruptions on Northern hemisphere summer temperature over the past 600 years. Nature 393, 450-455.
- Büntgen, U., Esper, J., Frank, D.C., Nicolussi, K., Schmidhalter, M., 2005. A 1052-year tree-ring proxy for alpine summer temperatures. Clim. Dyn. 25, 141–153.
- Büntgen, U., Frank, D.C., Nievergelt, D., Esper, J., 2006. Summer temperature variations in the european Alps, AD 755–2004. J. Clim. 19, 5606–5623.

Büntgen, U., Raible, C.C., Frank, D., Helama, S., Cunningham, L., Hofer, D., Esper, J., 2011a. Causes and consequences of past and projected scandinavian summer temperatures, 500–2100 AD. PLoS One 6, e25133.

- Büntgen, U., Tegel, W., Nicolussi, K., McCormick, M., Frank, D., Trouet, V., Esper, J., 2011b. 2500 years of European climate variability and human susceptibility. Science 331, 578–582.
- Büntgen, U., Frank, D., Neuenschwander, T., Esper, J., 2012. Fading temperature sensitivity of alpine tree growth at its Mediterranean margin and associated effects on large-scale climate reconstructions. Clim. Change 114, 651–666.
- Büntgen, U., Piermattei, A., Crivellaro, A., Reinig, F., Krusic, P.J., Trnka, M., Esper, J., 2022. Common era treeline fluctuations and their implications for climate reconstructions. Glob. Planet. Change 219, 103979.
- Cook, B.I., Cook, E.R., Anchukaitis, K.J., Singh, D., 2024. Characterizing the 2010 Russian heat wave – Pakistan flood concurrent extreme over the last millennium using the Great Eurasian drought Atlas. J. Clim. 37, 4389–4401.
- Cook, E.R., Kairiukstis, L.A. (Eds.), 1990. Methods of Dendrochronology: Applications in the Environmental Sciences. Kluwer, Dordrecht.
- Cook, E.R., Peters, K., 1997. Calculating unbiased tree-ring indices for the study of climatic and environmental change. Holocene 7, 361–370.
- Cook, E.R., Briffa, K.R., Jones, P.D., 1994. Spatial regression methods in dendroclimatology: a review and comparison of two techniques. Int. J. Clim. 14, 379–402.
- Esper, J., Cook, E.R., Krusic, P.J., Peters, K., Schweingruber, F.H., 2003. Tests of the RCS method for preserving low-frequency variability in long tree-ring chronologies. Tree-Ring Res. 59, 81–98.
- Esper, J., Frank, D.C., Wilson, R.J., Briffa, K.R., 2005. Effect of scaling and regression on reconstructed temperature amplitude for the past millennium. Geophys. Res. Lett. 32, 107711
- Esper, J., Büntgen, U., Frank, D.C., Nievergelt, D., Liebhold, A., 2007a. 1200 years of regular outbreaks in alpine insects. Proc. R. Soc. B 274, 671–679.
- Esper, J., Büntgen, U., Frank, D., Pichler, T., Nicolussi, K., 2007b. Updating the tyrol treering dataset. TRACE 5, 80–85.
- Esper, J., Frank, D., Büntgen, U., Verstege, A., Hantemirov, R.M., Kirdyanov, A.V., 2010. Trends and uncertainties in Siberian indicators of 20th century warming. Glob. Change Biol. 16, 386–398.
- Esper, J., Frank, D.C., Timonen, M., Zorita, E., Wilson, R.J., Luterbacher, J., Büntgen, U., 2012. Orbital forcing of tree-ring data. Nat. Clim. Change 2, 862–866.
- Esper, J., Schneider, L., Smerdon, J.E., Schöne, B.R., Büntgen, U., 2015. Signals and memory in tree-ring width and density data. Dendrochronologia 35, 62–70.
- Esper, J., Krusic, P.J., Ljungqvist, F.G., Luterbacher, J., Carrer, M., Cook, E., Büntgen, U., 2016. Ranking of tree-ring based temperature reconstructions of the past millennium. Ouat. Sci. Rev. 145, 134–151.
- Esper St., J., George, S., Anchukaitis, K., D'Arrigo, R., Ljungqvist, F.C., Luterbacher, J., Büntgen, U., 2018. Large-scale, millennial-length temperature reconstructions from tree-rings. Dendrochronologia 50, 81–90.
- Esper, J., Smerdon, J.E., Anchukaitis, K.J., Allen, K., Cook, E.R., D'Arrigo, R., Büntgen, U., 2024a. The IPCC's reductive common era temperature history. Comm. Earth Environ. 5, 222.
- Esper, J., Torbenson, M., Büntgen, U., 2024b. 2023 summer warmth unparalleled over the past 2000 years. Nature 631, 94–97.
- Frank, D., Esper, J., 2005. Characterization and climate response patterns of a highelevation, multi-species tree-ring network in the European Alps. Dendrochronologia 22, 107–121.
- Frank, D., Esper, J., Cook, E.R., 2007b. Adjustment for proxy number and coherence in a large-scale temperature reconstruction. Geophys. Res. Lett. 34. L16709.
- Frank, D., Büntgen, U., Böhm, R., Maugeri, M., Esper, J., 2007a. Warmer early instrumental measurements versus colder reconstructed temperatures: shooting at a moving target. Quat. Sci. Rev. 26, 3298–3310.
- Frank, D.C., Esper, J., Raible, C.C., Büntgen, U., Trouet, V., Stocker, B., Joos, F., 2010. Ensemble reconstruction constraints on the global carbon cycle sensitivity to climate. Nature 463, 527–530.
- Gao, S., Camarero, J.J., Babst, F., Liang, E., 2023. Global tree growth resilience to cold extremes following the tambora volcanic eruption. Nat. Commun. 14, 6616.
- Grudd, H., 2008. Torneträsk tree-ring width and density AD 500–2004: a test of climatic sensitivity and a new 1500-year reconstruction of north Fennoscandian summers. Clim. Dyn. 31, 843–857.
- Guillet, S., Corona, C., Stoffel, M., Khodri, M., Lavigne, F., Ortega, P., Oppenheimer, C., 2017. Climate response to the samalas volcanic eruption in 1257 revealed by proxy records. Nat. Geosci. 10, 123–128.
- Gunnarson, B.E., Linderholm, H.W., 2002. Low-frequency summer temperature variation in central Sweden since the tenth century inferred from tree rings. Holocene 12, 667–671.
- Harris, I., Osborn, T.J., Jones, P., Lister, D., 2020. Version 4 of the CRU TS monthly highresolution gridded multivariate climate dataset. Sci. Data 7, 109.
- Hildreth, W., Fierstein, J., 2012. The Novarupta-Katmai Eruption of 1912: Largest Eruption of the Twentieth Century: Centennial Perspectives. US Department of the Interior, US Geological Survey, Reston, VA, USA.
- Holmes, R.L., 1983. Computer-assisted quality control in tree-ring dating and measurement. Tree-Ring Bull. 43, 69–78.
- Johnson, D.M., Büntgen, U., Frank, D.C., Kausrud, K., Haynes, K.J., Liebhold, A.M., Stenseth, N.C., 2010. Climatic warming disrupts recurrent alpine insect outbreaks. Proc. Nat. Acad. Sci. 107, 20576–20581.
- King, A.D., Donat, M.G., Fischer, E.M., Hawkins, E., Alexander, L.V., Karoly, D.J., Perkins, S.E., 2015. The timing of anthropogenic emergence in simulated climate extremes. Environ. Res. Lett. 10, 094015.

- Kuhl, E., Esper, J., Schneider, L., Trouet, V., Kunz, M., Klippel, L., Hartl, C., 2024. Revising alpine summer temperatures since 881 CE. Clim. Dyn. 62, 6141–6157.
- Kunz, M., Esper, J., Kuhl, E., Schneider, L., Büntgen, U., Hartl, C., 2023. Combining treering width and density to separate the effects of climate variation and insect defoliation. Forests 14, 1478.
- Larocque-Tobler, I., Grosjean, M., Heiri, O., Trachsel, M., Kamenik, C., 2010. Thousand years of climate change reconstructed from chironomid subfossils preserved in varved lake Silvaplana, Engadine, Switzerland. Quat. Sci. Rev. 29, 1940–1949.
- Linderholm, H.W., Gunnarson, B.E., 2019. Were medieval warm-season temperatures in Jämtland, central Scandinavian Mountains, lower than previously estimated? Dendrochronologia 57, 125607.
- Ljungqvist, F.C., Piermattei, A., Seim, A., Krusic, P.J., Büntgen, U., He, M., Esper, J., 2020. Ranking of tree-ring based hydroclimate reconstructions of the past millennium. Quat. Sci. Rev. 230, 106074.
- Loader, N.J., Young, G.H.F., Grudd, H., McCarroll, D., 2013. Stable carbon isotopes from Torneträsk, Northern Sweden provide a millennial length reconstruction of summer sunshine and its relationship to Arctic circulation. Quat. Sci. Rev. 62, 97–113.
- Melvin, T.M., Grudd, H., Briffa, K.R., 2013. Potential bias in 'updating' tree-ring chronologies using regional curve standardization: re-processing 1500 years of Torneträsk density and ring-width data. Holocene 23, 364–373.
- Pretis, F., Schneider, L., Smerdon, J.E., Hendry, D.F., 2017. Detecting volcanic eruptions in temperature reconstructions by designed break-indicator saturation. In: Lin, B.C., Zheng, S. (Eds.), Environmental Economics and Sustainability. Wiley, Chichester, pp. 7–37.
- Riechelmann, D.F., Hartl, C., Esper, J., 2020. The effect of provenance of historical timber on tree-ring based temperature reconstructions in the Western Central Alps. IForest 13, 351–359.
- Riechelmann, D.F.C., Schmidhalter, M., Büntgen, U., Esper, J., 2013. Extending the high elevation larch ring width chronology from the simplon region in the Swiss Alps over the past millennium. TRACE 11, 103–107.

- Rohde, R., Muller, R.A., Jacobsen, R., Muller, E., Perlmutter, S., Rosenfeld, A., Wickham, C., 2013. A new estimate of the average earth surface land temperature spanning 1753–2011. Geoinf. Geostat. Overv. 1, 1.
- Schneider, L., Konter, O., Esper, J., Anchukaitis, K.J., 2023. Constraining the nineteenth-century temperature baseline for global warming. J. Clim. 36, 6261–6272.
- Schweingruber, F.H., Bräker, O.U., Schär, E., 1979. Dendroclimatic studies on conifers from central Europe and Great Britain. Boreas 8, 427–452.
- Serre, F., 1978. The dendroclimatological value of the European larch (*Larix decidua* Mill.) in the French Maritime Alps. Tree-Ring Bull. 38, 25–34.
- Sigl, M., Winstrup, M., McConnell, J.R., Welten, K.C., Plunkett, G., Ludlow, F., Woodruff, T.E., 2015. Timing and climate forcing of volcanic eruptions for the past 2500 years. Nature 523, 543–549.
- Tegel, W., Vanmoerkerke, J., Büntgen, U., 2010. Updating historical tree-ring records for climate reconstruction. Quat. Sci. Rev. 29, 1957–1959.
- Tejedor, E., Serrano-Notivoli, R., de Luis, M., Saz, M.A., Hartl, C., St. George, S., Esper, J., 2020. A global perspective on the climate-driven growth synchrony of neighboring trees. Glob. Ecol. Biogeogr. 29, 1114–1125.
- Tejedor, E., Benito, G., Serrano-Notivoli, R., González-Rouco, F., Esper, J., Büntgen, U., 2024. Recent heatwaves as a prelude to climate extremes in the Western Mediterranean region. npj Clim. Atmos. Sci. 7, 218.
- Toohey, M., Sigl, M., 2017. Volcanic stratospheric sulfur injections and aerosol optical depth from 500 BCE to 1900 CE. Earth Syst. Sci. Data 9, 809–831.
- Usoskin, I.G., 2017. A history of solar activity over millennia. Living Rev. Sol. Phys. 14,
- Wang, B., Luo, X., Yang, Y.M., Sun, W., Cane, M.A., Cai, W., Liu, J., 2019. Historical change of El Niño properties sheds light on future changes of extreme El Niño. Proc. Nat. Acad. Sci. 116, 22512–22517.
- Wanner, H., Pfister, C., Neukom, R., 2022. The variable European little ice age. Quat. Sci. Rev. 287, 107531.
- Wilson, R., Anchukaitis, K., Briffa, K.R., Büntgen, U., Cook, E., D'Arrigo, R., Zorita, E., 2016. Last millennium northern hemisphere summer temperatures from tree rings: Part I: the long term context. Quat. Sci. Rev. 134, 1–18.